

Measurements of Gravitational Attractions at small Accelerations

W. Bartel^{1†} C. W. Elvers¹ L. Jönsson² G. Kempf¹ H. Krause³
B. Loehr¹ E. Lohrmann³, H. Meyer^{4†} P. Steffen^{1*} E. Wuensch¹

¹Deutsches Elektronen-Synchrotron DESY, Hamburg, Germany

²Lund University, Sweden

³Universität Hamburg

⁴Bergische Universität, Wuppertal

[†]deceased

*corresponding author: peter.steffen@desy.de

Abstract

Gravitational interactions were studied by measuring the influence of small external field masses on a microwave resonator. It consisted of two spherical mirrors, which acted as independent pendulums individually suspended by strings. Two identical field masses were moved along the axis of the resonator symmetrically and periodically between a near and a far position. Their gravitational interaction altered the distance between the mirrors, changing the resonance frequency, which was measured and found consistent with Newton's law of gravity. The acceleration of a single mirror caused by the two field masses at the closest position varied from $5.4 \cdot 10^{-12} \text{ m/s}^2$ to $259 \cdot 10^{-12} \text{ m/s}^2$.

1 Introduction

In the 1930s, observations were made by several astronomers that the galaxies contain more mass than expected from Newton’s gravitational law, based on the visible mass. The first publication of such an observation was made by K. Lundmark [1]. Later the term “dark matter” was coined. The present predominant hypothesis is that dark matter is some kind of massive, stable, neutral, weakly interacting particle. However, in spite of many researches to find or identify the particles of dark matter, nothing has been found so far [2], [4]. An alternative to dark matter is the MOND-model that assumes a modified Newton’s law of gravity [3].

A high statistics dataset has been evaluated by S. S. McGaugh et al. [5], [16]. In the acceleration range of about $(20 - 500) 10^{-12} \text{ m/s}^2$ there is a clear deviation of the measured data from expectations obtained from Newton’s predictions based on the baryonic matter. This experiment aims to test Newton’s gravitational law at accelerations below 10^{-10} m/s^2 on Earth, relying solely on gravitational interactions.

Small field masses were used to accelerate the masses of two pendulums perpendicular to the Earth’s acceleration. The measured movements of the pendulums are proportional to the acceleration caused by the field masses.

Results from measurements with field masses ranging from 9 kg to 1 kg have been published previously [6] using an earlier version of the experiment. The results did not show any deviation from Newton’s law of gravitation. A similar result was obtained using an experimental setup of the Cavendish-type [7].

This paper presents results from an improved experimental setup using field masses from 3 kg to 0.1 kg, which extend the range of accelerations to significantly smaller values, measured with considerably higher precision. The measurements were carried out in the years 2020 to 2022.

2 Experimental Setup

Figure 1 shows the main components of the experiment: a system of two pendulums that form a microwave resonator, similar to a Fabry-Perot interferometer. The introduction of external field masses causes a tiny acceleration of the pendulums in the direction of the resonator axis. The resulting change of the resonator length caused a measurable change in the resonance frequency.

The resonator was located inside a vacuum vessel. A transport system

moved the field masses between positions A and B.

An earlier version of the apparatus had been built and operated at Wuppertal University for a precision measurement of the gravitational constant: [8], [9], [10], [11], where details can be found. It was later transferred to DESY to an experimental hall of the PETRA accelerator.

After an initial measurement period, which resulted in a publication [6], it was relocated to an underground experimental hall of the HERA accelerator, and the setup was improved significantly.

2.1 The Resonator

The central part of the experiment was a microwave resonator. Figure 2 shows a schematic view. It consisted of two mirrors with spherical surfaces and a cylindrical center piece in between, which suppresses higher order resonance modes. The mirrors are made of copper with a gold plated surface on the concave side. They were enclosed by an aluminum tubus. The mirrors and the center piece were suspended individually by thin strings of about 2.7 m in length from the upper lid of the vacuum vessel. The thin strings had a diameter of 0.2 mm and were made of a high density polyethylene (Dyneema). Each mirror acted as a mechanical pendulum with a period of 3.278 s. The resonator was operated at a mean resonance frequency of 23.2699 GHz. It was adjusted continuously to compensate slow drifts caused by changes of temperature and air pressure.

Stochastic movements of the pendulums were damped by permanent magnets positioned below the mirrors in order to optimize the performance of the resonator. The center of gravity of each mirror coincided with the vertex of the mirror. The distance between the two vertices was determined to $b_0 = 0.2400$ m. Radio frequency power was fed into the resonator through a small hole in the center of one mirror, and was similarly extracted on the opposite side. It was rectified and read out.

2.2 The Vacuum Vessel

In figure 1 a cryostat is shown. It was used as vacuum vessel at room temperature. It was a cylindrical stainless-steel tank with a removable lid on top. It was supported at the upper surface from a massive concrete structure. Ground vibrations were suppressed by a mechanical damping system.

The vacuum vessel was thermally shielded with a layer of Styrofoam. A removable, thermally insulating hood covered the top of the concrete

structure, maintaining the lid's temperature variation at about 0.1 degrees Celsius within a 12-hour period. Over longer time periods the temperature changes were about a factor of 10 higher, especially between summer and winter. At the height of the resonator the vacuum vessel was shielded against magnetic fields by a μ -metal cylinder. The lid of the vessel was leveled along and transverse to the resonator axis with a precision of a few micro rad. Variations of the lid's inclination occurred up to 10 μ rad.

Environmental changes of air pressure and temperature led to a drift of the resonance frequency of up to 10 kHz within a week.

2.3 The Transport System of the Field Masses

Two granite optical benches were located on opposite sides of the vacuum vessel along the centerline of the resonator. Both benches supported a transport system on which field masses were moved between a far and a near position (see figure 1). The distance between the two positions was always 2.683 m on either side.

The construction of the transport system allowed for a change in the near position on both benches. This flexibility enabled different gravitational accelerations on the mirrors with given field masses (for details, see section 4.3). Several spheres of different materials but with the same diameter of 0.127 m were used as field masses.

2.4 Improvements

After the relocation to an underground experimental hall of the HERA accelerator the experimental setup was significantly improved:

The lid inclination was stabilized by using a damped suspension of the vacuum vessel.

Temperature stability of the lid was maintained down to 0.1 degrees Celsius over several hours.

Stable vacuum conditions were maintained in the vessel at about $2 \cdot 10^{-5}$ mbar.

The method for determining the near positions of the field masses was improved,

The data acquisition was significantly improved by the installation of a recursive algorithm for the continuous readjustment to a drifting resonance frequency. This resulted in a more stable data collection process

independent of external large distortions, like earthquakes. Further on, it allowed to choose a resonance frequency with a narrower width resulting in an improved frequency resolution.

3 Predictions from Newton's Law of Gravitation

The size of the deflection of a pendulum is determined by the equilibrium between the gravitational attraction by the field masses and the restoring force of the Earth's gravitation.

For point masses, the gravitational force F between a field mass m and a pendulum with mass M at a distance of r is given by:

$$F = G \cdot \frac{m}{r^2} \cdot M \quad (1)$$

The acceleration of the pendulum by the field mass is

$$a(m, r) = G \cdot \frac{m}{r^2} \quad (2)$$

Two equal field masses were positioned symmetrically w.r.t. the resonator. They were alternated periodically between a near (r_n) and a far (r_f) position. Assuming point masses for field masses and mirrors, the change of the resonator length between these two positions is described by the formula

$$db_{\text{point}} = 2 \frac{G}{\omega_0^2} \cdot m \cdot \left(\left(\frac{1}{r_n^2} - \frac{1}{(r_n + b)^2} \right) - \left(\frac{1}{r_f^2} - \frac{1}{(r_f + b)^2} \right) \right) \quad (3)$$

where $\omega_0^2 = g/L$ is the frequency of a pendulum with the length L and g is the local gravitational field of Earth. b is the distance of the vertices as well as the centers of gravity of the two mirrors.

In terms of acceleration one has

$$db_{\text{point}} = \frac{2}{\omega_0^2} \left(\left(a(m, r_n) - a(m, r_n + b) \right) - \left(a(m, r_f) - a(m, r_f + b) \right) \right) \quad (4)$$

The field masses were homogeneous spheres, treated as point masses. However, the mirrors have a complicated geometric structure composed of different materials. The acceleration of the extended mirrors were calculated by numerical integration over the shapes of different densities:

$$a(m, r)_{\text{ext}} = G \cdot \frac{1}{M} \cdot \int_V \frac{\rho(V) \cdot m}{r(V)^2} dV, \quad (5)$$

where $\rho(V)$ is the density of the volume elements, and $r(V)$ is the distance of field mass and volume element projected onto the resonator axis.

Using $a(m, r)_{ext}$ in formula 4 gives the predicted result:

$$\begin{aligned} db_{pred} &= \frac{2}{\omega_0^2} \left(\left(a(m, r_n)_{ext} - a(m, r_n + b)_{ext} \right) \right. \\ &\quad \left. - \left(a(m, r_f)_{ext} - a(m, r_f + b)_{ext} \right) \right) \end{aligned} \quad (6)$$

The ratio of db_{pred} for extended and point masses ranges from 0.96 to 0.99. The contribution of the far position to db_{pred} is about 1%. It was neglected. Therefore the relevant acceleration on a single mirror by the two field masses in the near position is described by

$$a_{pred} = \frac{g}{L} \cdot \frac{db_{pred}}{2} \quad \text{and} \quad a_{meas} = \frac{g}{L} \cdot \frac{db_{meas}}{2}, \quad \text{resp.} \quad (7)$$

For the actual calculations the following values were used:

$$G = 66.7428 \cdot 10^{-12} \frac{\text{m}^3}{\text{kg s}^2} \quad [12]$$

$$g = 9.8138 \text{ m/s}^2 \quad [13]$$

4 Measuring Procedure

The aim of the experiment is to measure the gravitational effect of the two field masses on the mirrors of the resonator. This is determined from the resonance frequencies of near and far position data.

4.1 Frequencies of the Resonator

According to [14], the resonance frequencies of a cylindrical resonator with spherical mirrors are given by:

$$f = \frac{c}{2b} \cdot \left\{ q + \frac{n}{\pi} \arccos \left(1 - \frac{b}{R} \right) + \frac{N}{8\pi^2 Rk} + \mathcal{O}(10^{-4}) \right\} \quad (8)$$

where:

q = axial mode number.

p = radial mode number.

m = azimuthal mode number.

$$N = 2p^2 + 2pm - m^2 + 2p - 2 + m \pm 4m.$$

$$n = 2p + m + 1.$$

$R = 0.56$ m, the curvature radius of spherical mirrors.

c the speed of light.

$k = f / c$ the wave number.

Our experiment was performed at a resonance frequency with $p = m = 0$. The parameters q, p, m have been determined by a simultaneous fit of formula 8 to a series of resonances including the chosen one, where the axial mode number is 37.

The relation between db and its corresponding change in resonance frequency df is given by:

$$db = \beta \cdot df \quad \text{with} \quad (9)$$

$$\beta = -\frac{b}{f} \left(1 - \frac{n \cdot c}{2\pi \cdot f} \sqrt{\frac{1}{2Rb - b^2}} + \mathcal{O}(10^{-4}) \right). \quad (10)$$

For the used resonance frequency of 23.2699 GHz it results in $\beta = 10.371 \cdot 10^{-12} \text{ m/Hz}$. β is important for the conversion of the theoretically expected db to the expected df , the frequency difference expected for data with near and far field mass. It allows a direct comparison of predicted and measured values of df . This comparison requires an evaluation of the uncertainties of the used parameters. β depends essentially on the parameters f and b . The relative uncertainty of f , $\delta f/f$, was determined from the slow drift of the resonance frequencies around the average resonance frequency of the whole 2 1/2 year measuring period. It amounts to $\delta f/f < 0.2 \cdot 10^{-6}$. According to equation 8, the relative uncertainty of b is $\delta b/b = -\delta f/f$. Therefore the relative uncertainty of β is $\delta \beta/\beta \approx 2 \cdot \delta f/f < 0.4 \cdot 10^{-6}$.

These uncertainties are very small as compared to the results of measurements and theoretical predictions (see table 2). They were neglected in the numerical calculations of the theoretical predictions, where $b = b_0$ and $f = 23.2699$ GHz were assumed.

4.2 Determination of the Resonance Frequency

The resonance frequency, f_r , was determined from measurements of the resonator amplitudes at five equidistant frequencies (10 kHz difference). These

were adjusted continuously to center approximately around the slowly drifting resonance. These frequencies cover 30% of the resonance width at half maximum of the resonance shape (about 130 kHz).

A Lorentz curve is expected to describe the resonance shape:

$$U(f_i) = U_{\max} \cdot \frac{1}{1 + 4((f_i - f_r)/f_w)^2} \quad \text{for } i = 1 - 5 \quad (11)$$

The maximum amplitude U_{\max} , the width of the Lorentz curve f_w , and the resonance frequency f_r could be obtained from a fit of equation 11 to the 5 amplitude measurements $U(f_i)$.

However, the inverted Lorentz curve is a parabola that was used for a much faster fit:

$$U(f_i)^{-1} = a + b \cdot f_i + c \cdot f_i^2 \quad \text{for } i = 1 - 5, \quad \text{with} \quad (12)$$

$$f_r = -\frac{b}{2c} \quad (13)$$

The parabola fit was sufficiently fast for an online determination, and allowed an immediate adjustments of the measurement range to a drifting resonance frequency.

The resolution $\sigma(U(f_i))$ was about 0.05 mV. The resolution of the resonance frequency benefited from the improved data acquisition system (see section 2.4).

4.3 Field Masses

The used field masses were spheres of different materials and mass values, each with a diameter of 0.127 m, as specified in the table below.

material	marble	plastic	plastic	plastic
mass	2.92 kg	1.002 kg	0.294 kg	0.116 kg
accuracy	± 0.1 g	± 0.1 g	± 0.1 g	± 0.1 g
structure	solid	solid	hollow	hollow

Measurements were performed with different configurations of field masses and distances between the gravity centers of the field mass and the closer mirror as specified in the table below:

mass [kg]	0.116	0.294	0.116	0.294	0.294	1.002	2.924
r_n [m]	0.7537	1.0127	0.5932	0.7537	0.5932	0.5932	0.5932

The positions of the two field masses were changed every half an hour from their far positions to their near positions and vice versa. About 5000 measurements of the resonance frequency were registered per half hour period. The duration of data collection for each configuration ranged from 500 to 1000 hours.

5 Systematic Effects

Two categories of systematic uncertainties affect the comparison of the results with the expectations from Newton's Law of gravitation.

The first category consists of effects that might or do influence the determination of the resonance frequency:

The frequency stability of the radio frequency generator output was compared to a Rubidium Standard frequency. No difference was found that would influence the resonator frequency determinations.

The removable cover of the vacuum vessel behaved like a membrane. External influences, such as temperature and pressure, led to changes of the resonance frequency. In section 7.1 it is described how this was treated in the analyses of the data.

Measurements with no movement of the field masses were performed to test whether there is a bias in the measurement procedure and the analysis methods. The result $df = -0.058 \pm 0.063$ Hz is compatible with zero. This result was obtained following the analysis procedures described in section 7.

The second category of uncertainties is associated with the calculation of expectations from Newton's law of gravity.

A possible asymmetry of the resonator position in the experimental setup was determined using two methods:

Measurements starting with one field masses in the near position and the other in the far position. These positions were exchanged every 0.5 h.

Measurements with only one single field mass on one side, alternating between the far and near position. A second set of measurements were performed with the same field mass on the opposite side.

Both methods resulted in an asymmetric position of the resonator of about 5 mm. The asymmetry effect almost completely cancels when two field masses are used. The remaining deviation amounts to a negligible 0.03 % change of df .

The distances between the centers of gravity of the field masses to the centers of gravity of the mirrors play a critical role in the calculation of the expectation from Newton's law. The distances in the near position could not be measured directly because the resonator was located in the vacuum vessel between the field-masses. Instead, the distance, D , between the centers of the two field masses in the near position was measured to be $D = 1.4270 \pm 0.0005$ m, resulting in

$$r_n = \frac{1}{2}(D - b_0) = 0.5935 \text{ m} . \quad (14)$$

The difference between the near and far position of the field masses was always 2.683 ± 0.003 m. The contribution of the masses in the far position was about 1 % of the total df . Therefore the uncertainty of the far position is negligible.

The field masses were measured with an electronic scale with an uncertainty of 0.1 g. Small differences between the field mass pairs cancel completely in the calculation of the prediction of df if the average of the two field masses are used.

The horizontal and vertical alignments of the field masses transport systems at the near positions deviate by at most 2 mm from the axis of the resonator. This has a negligible effect on the determination of df .

The accuracy of the predicted db_{pred} depends, according to equation 6, on $1/\omega_0^2 = L/g$, which depends on L , the pendulum length. This length has been measured to be 2.671 ± 0.001 m. The resulting relative uncertainty in the calculation of db_{pred} can be neglected.

6 Raw Data

The mirrors are permanently excited by vibrations of the ground floor resulting in oscillations of the resonance frequency. These vibrations added to the gravitational effects of the field masses in near and far positions. Figure 3 shows the originally determined resonance frequencies over a time interval

of 40 s. The frequencies given on the y-axis are obtained after subtraction of a constant offset. Single frequencies are shown as dots.

The bandwidth of the resonance frequencies is primarily dominated by pendulum oscillations, resulting from relative distance changes between the two mirrors. The pendulum period of approximately 3 s is clearly visible, as well as the data taking period of about 0.3 s. The resonance frequencies were filtered by averaging them over 30 to 60 second intervals (10 - 20 pendulum periods). During these intervals, the pendulum effect averages out.

The left-over averaged resonance frequencies are shown as black dots in figure 4 over a 2.5 hour span. They show a slow drift of the resonance frequency (see section 2.2). A frequency step occurs between half-hour intervals when the field masses alternate between near and far positions. The frequency fluctuations form a band with a standard deviation of about 5 Hz around the drifting resonance frequency.

Only the averaged and offset subtracted resonance frequencies were used in the further analysis of the data.

7 Data Analyses

Four data analysis methods were developed separately. In general the least square method was used for all fits, unless otherwise stated.

7.1 Different Analysis Methods

Independent methods (m = a,b,c,d) were developed for the analyses of the data. All analyses begin with the data selection:

Strong temporary distortions like earthquakes etc. were eliminated by visual inspection (a, b) or by a programmed procedure (c, d).

The methods used time intervals of 1 to 10 hours for the determination of initial results of df and their statistical uncertainties, taking into account the slow frequency drift.

The different methods are:

Method a: Time intervals of 10 hours were used. The slow frequency drift is described by a 5th order polynomial, that was fit to the frequencies of the periods with field masses in the far position. The residuals of the fit for near and far periods are two nearly Gaussian distributions: one for the near position data and one for the far position data. df is the difference of the two means. The uncertainty of df follows from the statistical uncertainty of the two means.

As an example, figure 5 shows distributions of the residuals of the 5th order polynomial fit to a selected 10-hour data-taking period, one for the field masses in the near position(dotted histogram) and one for the far position (solid histogram). The Gaussian fits of the histograms resulted in χ^2/ndf close to one. These demonstrate also the accurate description of the slow drift by the 5th order polynomial fit.

Method b: A parabola plus a rectangular function was fit to the resonance frequencies for 3 consecutive periods. The fit step-size of the rectangular function df and its statistical uncertainty were obtained from the fit.

Method c: As shown in figure 4, a parabola was fit to the frequencies of 3 consecutive periods with the same position of the field masses. The green line of the parabola describes the slow frequency drift with sufficient accuracy. The values of the parabola have been subtracted from the data. A rectangular function were fit to the resulting residuals of 1 hours data giving the step-size df and its statistical uncertainty. The fit result is shown as red line on top of the parabola in the figure.

Method d: A 5th order polynomial plus a rectangular wave were fit to all frequencies of a time intervals of 10 hours. The parameters of the polynomial describe the slow frequency drift. The rectangular wave changes its sign at every alternation between near and far position. The average step-size of the rectangular wave df and its statistical uncertainty was obtained from the fit.

For each method the initial results were combined to averages $df_m \pm \sigma df_m$ for each configuration of field masses and near distance. Table 1 shows the results of the different methods in columns 2 to 5 together with the predicted acceleration in column 1.

7.2 Combination of the four Methods

The mean value \overline{df} of the methods as well as its statistical uncertainty σ_{stat} were computed as weighted averages of the df_m and the σdf_m :

$$\overline{df} = \left(\sum_m df_m \cdot (\sigma df_m)^{-2} \right) / \left(\sum_m (\sigma df_m)^{-2} \right) \quad (15)$$

$$\sigma_{\text{stat}} = \left(\sum_m \sigma df_m \cdot (\sigma df_m)^{-2} \right) / \left(\sum_m (\sigma df_m)^{-2} \right) \quad (16)$$

Figure 6 shows the differences $(df_m \pm \sigma df_m) - \overline{df}$ for the different accelerations, demonstrating good agreement of the results from different analysis methods.

The standard deviation of \overline{df} describes the spread of the method results df_m around the mean \overline{df} . It is used as additional systematic uncertainty, σ_{sys} , for the difference between the four methods. Table 1 presents \overline{df} , as well as σ_{stat} and σ_{sys} in columns 6.

The combined uncertainty is

$$\delta\overline{df} = \sqrt{\sigma_{\text{stat}}^2 + \sigma_{\text{sys}}^2}. \quad (17)$$

8 Results

Table 2 gives $\overline{df} \pm \delta\overline{df}$ in column 1 for the different accelerations. The results for \overline{df} have uncertainties that are nearly the same for the different accelerations: the mean uncertainty is $\overline{\delta\overline{df}} = 0.074$ Hz. At the lowest acceleration \overline{df} could be determined with a significance of $3.5 \cdot \delta\overline{df}$. Therefore measurements at lower acceleration would have given only insignificant results.

The predictions of Newton's law, $df_N \pm \delta df_N$, are displayed in table 2 column 3. The uncertainties δdf_N were determined from the uncertainty of r_n .

The differences of measurement results and predictions, $\Delta df \pm \delta \Delta df$, are given in table 2 columns 5 for the different accelerations. Measurements and predictions agree well within the uncertainties. This is shown in in figure 7 by the red symbols.

Also shown, as black symbols, are the results of an earlier publication [6]. These were determined from the information taken from [15] on which the publication was based. It demonstrates the large improvement in accuracy and the extended acceleration range that has been obtained since the previous publication.

The accelerations on a single mirror were calculated using equations 7 and 9 for the measured accelerations and the Newtonian predictions and their corresponding uncertainties. The results are shown in table 2 in columns 2 and 4. In figure 8 the measured accelerations are displayed versus the predictions from Newton's Law. The data are in good agreement with the predictions. The latter are indicated by the solid line. Also shown are results from reference [7]. They agree well with the data of this experiment. The numerical values plotted here are not given in [7] but were provided by the authors as private communication. For comparison figure 8 contains in

addition the astronomical data provided by S. S. McGaugh [5], [16]. For these data the predictions for the expected accelerations are based on the known baryonic matter.

9 Discussion

The results of this experiment agree well with Newton's Law for accelerations down to 10^{-12} m/s². This is not the case for astronomical data where a significant discrepancy is observed for accelerations $< 10^{-10}$ m/s² as shown in figure 8. This does not indicate that measurements on Earth contradict models and theories which explain the astronomical data. The discrepancy between measured and expected accelerations demonstrates that the baryonic matter alone is not sufficient to describe the measured results.

Dark matter models explain data from regions in universe which are not dominated by gravitational effects of baryonic matter. This is not the case on Earth where gravitational effects are dominated by baryonic matter. In figure 8 the predicted accelerations for astronomical data are calculated for baryonic matter only. Dark matter causes additional gravitational acceleration. In the region of small baryonic acceleration, the presence of dark matter leads to higher predictions for the accelerations and may lead to an agreement with Newton's Law.

The MOND model has been formulated for regions where the gravitational potential is very small which practically eliminates external forces. This condition is not fulfilled on Earth. Therefore, the results of this experiments can neither prove nor disprove models and theories which are based on MOND.

10 Acknowledgment

We thank the DESY Directorate and the IT-division for their constant support. We are grateful for the assistance of the technical groups of DESY for their help and advice on many technical questions. Additionally we acknowledge the contributions of A. Brüdgam, S. Fleig, Y. Holler, T. Külper, S. Karstensen, and U. Packeiser in setting up the experiment. We express our gratitude for the fruitful discussions with the late N. Klein, W. Buchmüller, S. Glazov, C. Niebuhr, M. Takahashi, K. Schmidt-Hoberg, and A. Ringwald. We thank S. S. McGaugh for providing the astronomical data and S. Little and M. Little for providing the numerical values of their results.

References

- [1] K. Lundmark, *Über die Bestimmung der Entfernungen, Dimensionen, Massen und Dichtigkeit für die nächstgelegenen anagalactischen Sternsysteme*, Meddelanden från Lunds Astronomiska Observatorium Series I. 125: 1 - 13, 1930
- [2] L. Baudis, *The Search for Dark Matter*, arXiv:1801.08128v1
- [3] M. Milgrom, *A modification of the Newtonian dynamics as a possible alternative to the hidden mass hypothesis*, *Astrophys.J.*270(1983)365
- [4] M. J. Zurovski, Univ. Toronto , *38th International Cosmic Ray Conference, Dark Matter at ICRC 2023* arXiv:2309.12983v1
- [5] S. S. McGaugh, F. Lelli, J. M. Schombert, *The Radial Acceleration Relation in Rotationally Supported Galaxies*, *PRL* 17, 201101
- [6] H. Meyer et al, *Test of the Law of Gravitation at small Accelerations*, *Gen.Rel.Grav.* 44(2012) 2537-2545
- [7] S. Little and M. Little, *Laboratory test of Newton's law of gravity for small accelerations*, *Class. Quant. Grav.* 31 (2014) no.19, 195008, doi:10.1088/0264-9381/31/19/195008
- [8] J. Schurr, *A new method to test the gravitational law of Newton*, Dissertation, Bergische Universität Wuppertal, 1992
- [9] H. Walesch, *Test des Newtonschen Gravitationsgesetzes und die präzise Bestimmung von G*, Dissertation, Bergische Universität Wuppertal, 1995
- [10] A. Schuhmacher, *Systematische Untersuchungen zur Messung der Newtonschen Gravitationskonstanten mit einem Pendelresonator*, Dissertation, Bergische Universität Wuppertal, 1999
- [11] U. Kleinevoss, *Bestimmung der Newtonschen Gravitationskonstanten G*, Dissertation, Bergische Universität Wuppertal, 2001
- [12] E. Tiesinga, *CODATA recommended values of the fundamental physical constants: 2018*, *Rev.Mod.Phys.*93,0250
- [13] PTB National Metrology Institute of Germany, <https://www.ptb.de>

- [14] Kwai-Man Luk and Ping-Kong Yu, *Complex-source-point-theory of Gaussian Beams and Resonators*, IEE Proceedings, Vol 132, Issue 2, 105 - 113, doi:10.1049/ip-j.1985.0021
- [15] S. Schubert, *An experimental Test of Newton's Law of Gravitation for small Accelerations*, Dissertation, Universität Hamburg, 2011
- [16] S. S. McGaugh et al, <http://astroweb.case.edu/SPARC/>,
binned data: <http://astroweb.case.edu/SPARC/RARbins.mrt>,
SPARC, May 2020 12

a_{pred} [10^{-12} m/s ²]	df_a [Hz] σdf_a	df_b [Hz] σdf_b	df_c [Hz] σdf_c	df_d [Hz] σdf_d	\overline{df} [Hz] σ_{stat} σ_{syst}
5.4	0.520 0.080	0.390 0.090	0.312 0.054	0.364 0.082	0.377 0.070 0.078
6.2	0.230 0.090	0.358 0.060	0.297 0.045	0.229 0.067	0.291 0.058 0.048
10.2	0.691 0.043	0.749 0.039	0.639 0.031	0.648 0.046	0.677 0.038 0.044
13.8	0.870 0.090	0.689 0.063	0.736 0.044	0.721 0.064	0.737 0.058 0.050
25.9	1.380 0.041	1.477 0.076	1.362 0.045	1.347 0.057	1.379 0.049 0.037
88.5	4.570 0.050	4.513 0.136	4.618 0.048	4.696 0.076	4.608 0.058 0.048
258.6	13.512 0.070	13.447 0.088	13.550 0.040	13.576 0.051	13.542 0.052 0.037

Table 1: Results and uncertainties of the 4 methods are listed in columns 2 to 5 for the different a_{pred} . The combined results with statistical and systematic uncertainties are listed in column 6.

\overline{df} [Hz] $\delta\overline{df}$	a_{meas} δa_{meas}	df_N [Hz] δdf_N	a_{pred} δa_{pred}	Δdf [Hz] $\delta\Delta df$
0.377 0.105	7.2 2.0	0.286 0.0004	5.4 0.0	0.091 0.105
0.291 0.075	5.5 1.4	0.324 0.0004	6.2 0.0	-0.033 0.075
0.677 0.058	12.9 1.1	0.538 0.0009	10.2 0.0	0.139 0.058
0.737 0.076	14.0 1.4	0.726 0.0010	13.8 0.0	0.011 0.076
1.379 0.061	26.2 1.2	1.365 0.0022	25.9 0.0	0.014 0.061
4.608 0.075	87.6 1.4	4.655 0.0076	88.5 0.0	-0.047 0.075
13.542 0.064	257.5 1.2	13.600 0.0211	258.6 0.0	-0.059 0.068

Table 2: The combined results for \overline{df} and the corresponding accelerations, a_{meas} , the prediction, df_N , and their corresponding acceleration a_{pred} , and their difference Δdf are listed, together with the corresponding uncertainties.

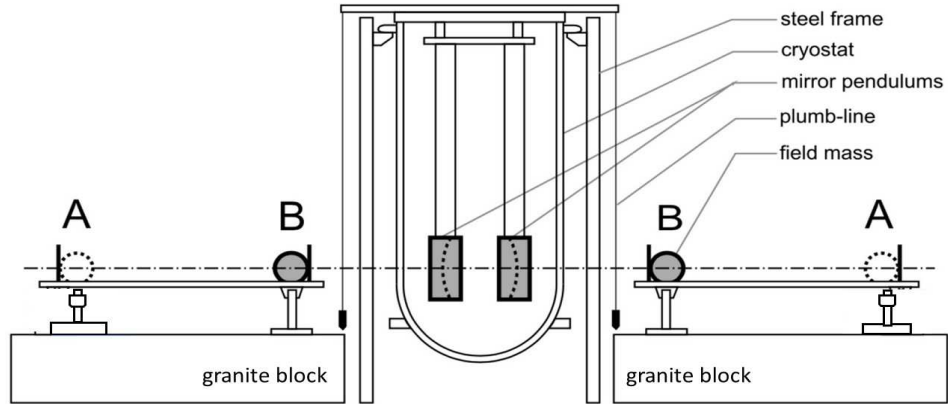


Figure 1: Detector scheme: two mirror pendulums which are pulled apart by the gravitational forces of field masses on both sides. The field masses change their positions between A and B.

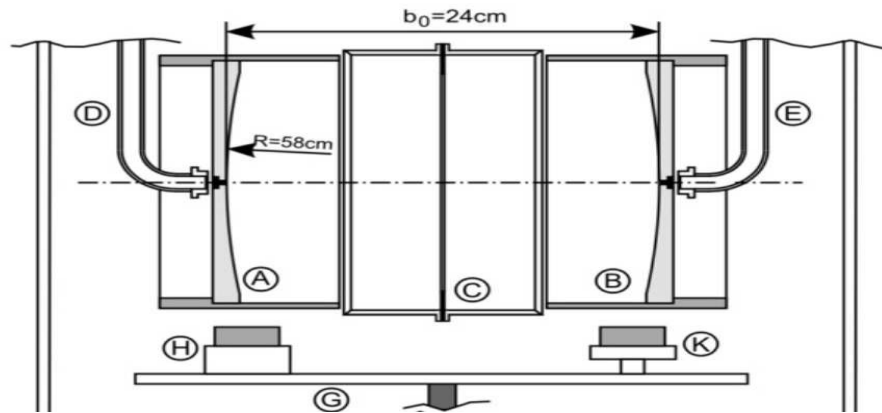


Figure 2: Resonator scheme: the two cylindrical mirror pendulums (A, B) form a microwave resonator together with a cylindrical mode filter (C) in between. The mode filter suppresses higher mode resonances. The radio frequency power is fed into the resonator via the wave guide (D). The resonator amplitude is measured at the opposite side (E). Oscillations of the pendulums are damped by independently adjustable magnets (H, K) on a movable table (G).

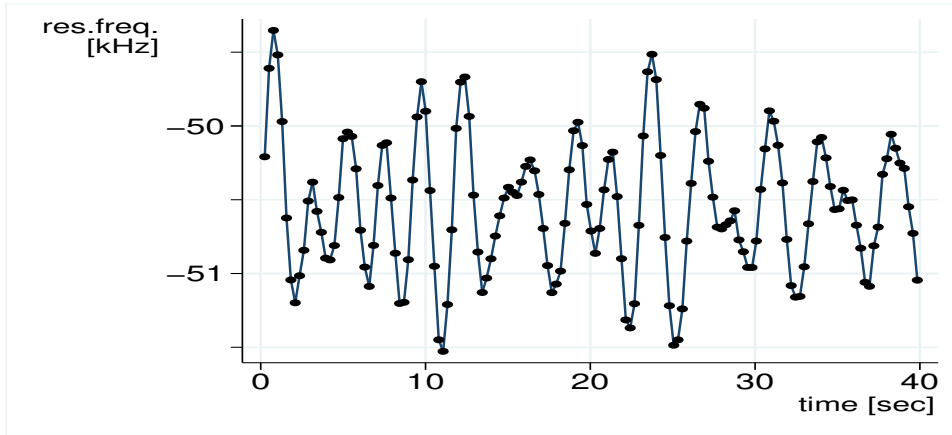


Figure 3: The points show the resonance frequencies for a time period of about 40 sec, after a fixed offset was subtracted. They were connected by straight lines to demonstrate clearly the effect of pendulum oscillations.

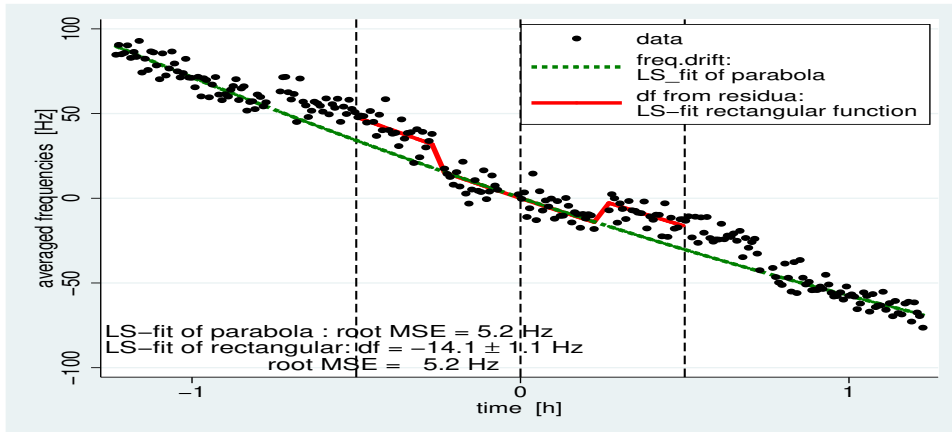


Figure 4: The points show the means of the resonance frequencies, averaged over 30 sec, for a time interval of 2.5 h. A fixed offset was subtracted from the frequencies as well as for the horizontal time axis. The data were derived from measurements with 2.924 kg field masses. A slow drift of the frequency of about 150 Hz is observed within the 2.5 h time interval, as described by the green line. Every half hour, a frequency step is observed originating from the position change of the field masses, described by the red line.

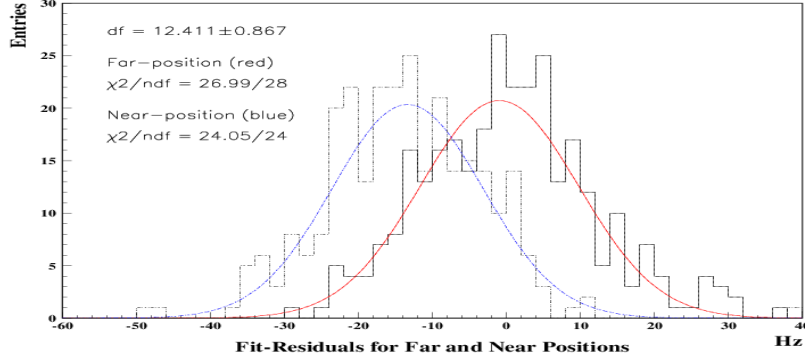


Figure 5: Shown are two histograms of the residuals of a 5th order polynomial fit to a selected 10-hour data-taking period, one for the field masses in the near position(dashed histogram), one for the far position(solid histogram). Gaussian curves were fitted to the histograms in blue and red. The resulting values of χ^2/ndf are close to one, demonstrating the goodness of the Gaussian fit. These also demonstrate the accurate description of the slow frequency drift by the 5th order polynomial fit.

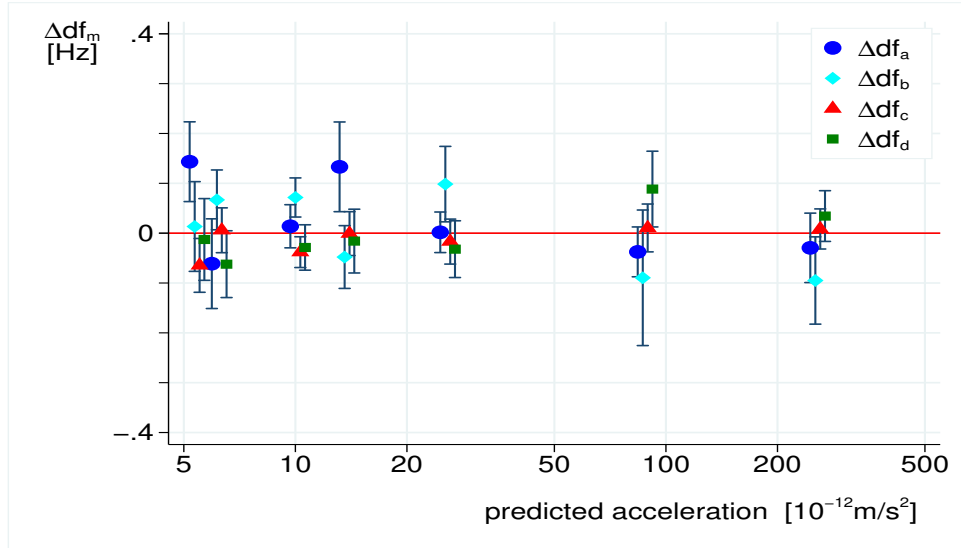


Figure 6: The differences $\Delta df_m = (df_m \pm \delta df_m) - \overline{df}$ of the different methods are shown for the predicted accelerations. They are presented slightly displaced for better visibility.

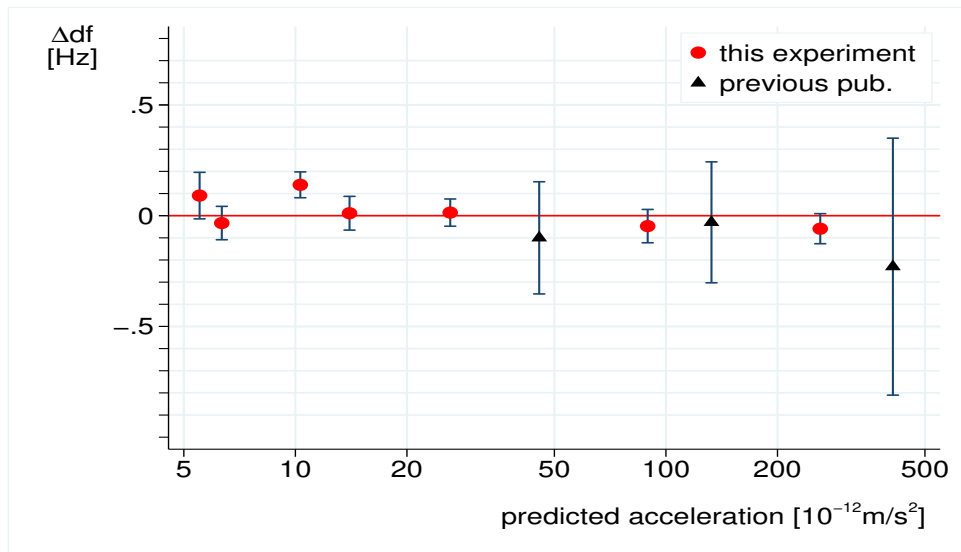


Figure 7: Differences, $\Delta df = \overline{df} - df_N$, of average results and predictions are shown for the predicted accelerations. The vertical error bars include the uncertainties of measurement and prediction. The red symbols show the results of this experiment. The black symbols show the results derived from the previous publication.

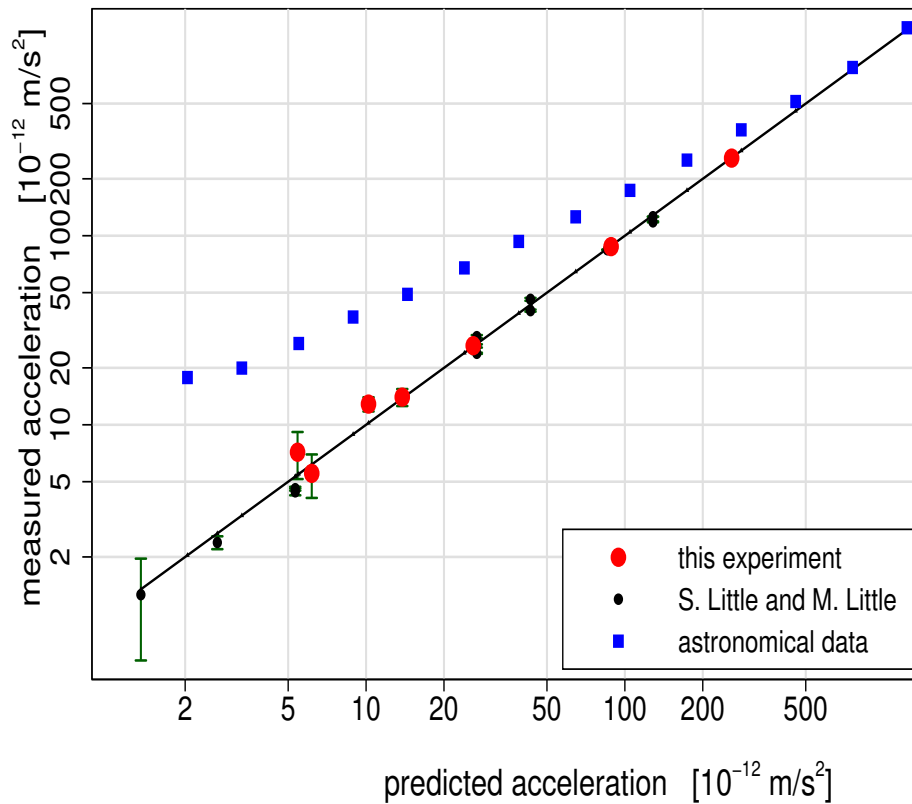


Figure 8: Comparison of measured and predicted acceleration of this experiment (red dots). The relative uncertainty of the predicted acceleration is about 0.14%. The black line indicates the equality of the two accelerations. The black symbols show the results from a previous publication [7]. The results of this experiment are compared to astronomical measurements [16] (blue squares); vertical axis: radial accelerations by galaxies measured at the boundaries; horizontal axis: predicted acceleration by the baryonic mass according to Newton's law. The uncertainties of the astronomical data are within the size of the symbols.